Atmospheric
Measurement
Techniques
Discussions

Light scattering at small angles by atmospheric irregular particles: modelling and laboratory measurements

T. Lurton[1], J.-B. Renard[1], D. Vignelles[1], M. Jeannot[1], R. Akiki[2], J.-L. Mineau[2,†], and T. Tonnelier[2]

[1]Laboratoire de Physique et Chimie de l'Environnement et de l'Espace, UMR7328, CNRS – 3A, avenue de la Recherche Scientifique, 45071 Orléans, France
[2]Environnement S. A., 111, boulevard Maximilien-Robespierre, 78300 Poissy, France
[†]deceased

AMTD

6, 7565–7591, 2013

Light scattering at small angles by irregular particles

T. Lurton et al.

Title Page

Abstract	Introduction
Conclusions	References
Tables	Figures

|◄ | ►|
◄ | ►

Back | Close

Full Screen / Esc

Printer-friendly Version

Interactive Discussion

Abstract

We investigated the behaviour of light scattering by particulates of various sizes (0.1 µm to 100 µm) at a small scattering angle. It was previously shown that for a small angle, the scattered intensities are weakly dependent upon the particulates' nature (Renard et al., 2010). Particles found in the atmosphere exhibit roughness that leads to large discrepancies with the classical Mie solution in terms of scattered intensities in the low angular set-up. This article focuses on building an effective theoretical tool to predict the behaviour of light scattering by real particulates at a small scattering angle.

We expose both the classical Mie theory and an adaptation to the case of rough particulates with a fairly simple roughness parametrisation. An experimental device was built, corresponding to the angular set-up of interest (low scattering angle and therefore low angular aperture), and measurements are presented that confirm the theoretical results with a good agreement. It is found that the differences between the classical Mie solution and actual measurements, especially for large particulates, can be attributed to the roughness of particulates.

It is also found that, in this low angular set-up, saturation of the scattered intensities occurs for relatively small values of the roughness parameter. This confirms the low variability in the scattered intensities for particulates of different kinds.

A direct interest of this study is a broadening of the dynamic range of optical counters: using a small angle of aperture for measurements allows greater dynamics in terms of particle size, and thus enables a single device to observe a broad range of particle sizes whilst utilising the same electronics.

1 Introduction

The importance of measuring the concentrations and masses of aerosols in the atmosphere has been highlighted by various studies (Zemp et al., 1999; Brunekreef and Holgate, 2002), given the possible effect of their presence in the ambient air upon

human health. A public directive on air quality was published (European Parliament, 2008) in order to establish standards for the protection of human health; in this context, the observation of aerosols appears of great relevance, and should be made in accordance to the established norms. Particulate matter (PM) is commonly classified in size bins – PM_{10} standing for example for particulates of aerodynamic size less than to 10 µm. Due to the large variety in the nature and size of the particulates as found in the environment, and their related properties and impacts, it is of utmost importance to distinguish between those different classes.

In order to monitor aerosols, optical particle counters (OPC) can be utilised. Their principle relies on the scattering of light by small particulates: an incident monochromatic laser beam is directed towards the particulates and scattered in space, a phenomenon which is fairly well described by Mie's theory (Mie, 1908) and in which the intensity of the scattered light strongly depends on the scattering angle of observation. Parameters such as the refractive index, the size of the particulate and its shape are key factors in the scattering process. In an OPC, the light flux is collected at a defined angle in order to yield information about the particulates. One can thus retrieve the size of the particulates, under certain assumptions upon their refractive index and shape (Dick et al., 1994). Standard OPCs are able to deliver both the concentrations and size distributions of the particulates as a continuous and real-time operating system (Rosen, 1964; Deshler et al., 2003; Donateo et al., 2006; Fischer and Koshland, 2006; McMurry, 2000; Renard et al., 2008, 2010). An example of an OPC is STAC (Stratospheric and Tropospheric Aerosols Counter). This device, dedicated to balloon flights, is operated by the LPC2E and works at a large scattering angle (70°) and under a broad field of view (70°); it is able to yield concentration profiles for particulates of diameters greater than 0.35 µm (liquid) and 1 µm (solid). It is also possible to place detectors at several angles at a same time (Eidhammer et al., 2008), enabling cross-comparison: depending on the angle, the scattered flux shall be more or less sensitive to either the nature or size of the particulate. At low scattering angles, below 20°, the

Title Page

Abstract | Introduction

Conclusions | References

Tables | Figures

◀ | ▶

◀ | ▶

Back | Close

Full Screen / Esc

Printer-friendly Version

Interactive Discussion

scattered light has a much stronger dependence on the particulates' size than on their nature (Renard et al., 2010).

Because real atmospheric particulates are not strictly spherical, the classical Mie solution cannot be assumed to be wholly valid as a scattering model; the roughness of the particulates has an impact on the scattered fluxes.

The global aim of this article is to study light scattering by irregular particulates at a small angle. Two main points should be immediately emphasised: first, given the weak dependence on the particulates' nature, this type of measurement yields first and foremost information upon the size of the particulates, which constitutes the practical application of such measurements; secondly, a low scattering angle naturally entails a narrow field of view. In a first part of this paper, we present a theoretical model for the scattering by irregular particulates. Then, we confirm the model by measurements. Some discussion follows, and some conclusions and perspectives are eventually drawn for practical aerosol monitoring applications.

2 Mie scattering for regular and irregular particulates

2.1 Classical Mie solution

The complete Mie scattering solution, introduced by Gustav Mie in 1908 (Mie, 1908) and later formalised in a more concise way through the use of Bessel functions (van de Hulst, 1957), is on the one hand rather long to detail comprehensively, and on the other hand well known in its basic aspects. Therefore, we will only point out the main facts of interest for this study.

For a unit-amplitude incident light of wavenumber k over a spherical particle, the scattered far field E_s expressed in spherical coordinates r, θ and ϕ can be expressed

as (van de Hulst, 1957):

$$E_{s\theta}(r,\theta,\phi) = -\frac{e^{-ikr}}{ikr}\cos\phi S_2(\theta) \tag{1}$$

$$E_{s\phi}(r,\theta,\phi) = \frac{e^{-ikr}}{ikr}\sin\phi S_1(\theta) \tag{2}$$

The E_{sr} radial component is assumed to be null.

The expressions of $S_1(\theta)$ and $S_2(\theta)$ are the following:

$$S_1(\theta) = \sum_{n=1}^{+\infty} \frac{2n+1}{n(n+1)}[a_n\pi_n(\cos\theta) + b_n\tau_n(\cos\theta)] \tag{3}$$

$$S_2(\theta) = \sum_{n=1}^{+\infty} \frac{2n+1}{n(n+1)}[b_n\pi_n(\cos\theta) + a_n\tau_n(\cos\theta)] \tag{4}$$

where the a_n and b_n series are the usual Mie coefficients, and the π_n and τ_n functions are angular polynomials, the expressions of which are detailed in (van de Hulst, 1957).

One shall note that Eqs. (3) and (4) depict an infinite series of terms, whose computation can of course not be carried out in its entirety. In order to compute values of S_1 and S_2 in simulations, one has to truncate the sum. A maximal running order is thus defined:

$$N_{max} = x + 4.3x^{\frac{1}{3}} + 1 \tag{5}$$

where x is the classical Mie particle parameter, $x = \frac{2\pi}{\lambda}a$ with a the radius of the particle. The sums carried out up to this order yield a maximal error of 10^{-8} upon the results; this formula finds justification on both empirical (Wiscombe, 1980; Mackowski et al., 1990) and theoretical grounds (Cachorro and Salcedo, 1991).

To yield the scattered light intensity at angles θ and ϕ and at a distance r, one simply sums up the squared expressions given in Eq. (1):

$$I_s(r, \theta, \phi) = \frac{I_0}{k^2 r^2} \left(|S_1(\theta)|^2 \sin^2 \phi + |S_2(\theta)|^2 \cos^2 \phi \right) \tag{6}$$

Because we are in our study dealing with small angles, we can consider that $|S_1(\theta)|^2$ and $|S_2(\theta)|^2$ do not differ greatly. Therefore, we can write:

$$I_s(r, \theta) \approx \frac{I_0}{k^2 r^2} \left(|S_1(\theta)|^2 + |S_2(\theta)|^2 \right) \tag{7}$$

2.2 Scattering by irregular particulates

Methods do exist to thoroughly model light scattering by irregular particulates (Penttilä et al., 2003; Muñoz et al., 2007), but it is necessary to have an a priori knowledge of the shape and nature of the particulates studied; conversely, our study uses all types of particulates, which is a hindrance to such traditional techniques. We propose to use a simplified method to simulate light scattering by irregular particulates. The simulation scheme we use is sufficient to show that the roughness of particulates has an effect upon the scattered fluxes, for a small scattering angle, a small angular aperture and for large particulate sizes. It will be shown that, as long as some moderate roughness is assumed over the particulates studied, and for the specific low angular measurement configuration, the nature of the particulate ultimately has no observable impact over the fluxes measured; the size of the particulate is then the only parameter to affect the scattered intensity.

We rely on Drossart's works (Drossart, 1990) on the one hand, and a classical diffraction approach on the other hand. In the article (Drossart, 1990), a model is described to derive a statistical expression of scattered intensities for irregular particulates; the diffracted part of the signal is treated in our study through a Monte-Carlo iteration process, and is used in the forward diffraction approximation realm.

2.2.1 Scattering by irregular particulates

In Drossart (1990), the intensity scattered by a rough particle is investigated, and a statistical model is derived to account for irregularities of the particle shape in the scattered intensity. The method is based on using a weighting between the classical Mie solution, and incoherent scattered intensities due to the random aspect of the phases of the scattered signals.

In order to lighten the notation and to concentrate on the points of interest, we remove the distance factor from the equations; they were nonetheless taken into consideration when using the model to perform our simulations.

We have thus on the one hand the coherent scattered intensities, corresponding to the classical Mie solution:

$$I^0_{(1,2)}(\theta) = |S_{(1,2)}(\theta)|^2 \tag{8}$$

and on the other hand incoherent scattered intensities, due to the surface roughness of the particle and the random phase distribution induced:

$$I^\infty_1(\theta) = \sum_{n=1}^{+\infty} \left(\frac{2n+1}{n(n+1)} \right)^2 |a_n \pi_n(\cos\theta) + b_n \tau_n(\cos\theta)|^2 \tag{9}$$

$$I^\infty_2(\theta) = \sum_{n=1}^{+\infty} \left(\frac{2n+1}{n(n+1)} \right)^2 |b_n \pi_n(\cos\theta) + a_n \tau_n(\cos\theta)|^2 \tag{10}$$

In Drossart (1990), the weighting of the two kinds of functions is made using a factor f to yield the total scattered intensities:

$$I_{(1,2)}(\theta) = f I^0_{(1,2)}(\theta) + (1-f) I^\infty_{(1,2)}(\theta) \tag{11}$$

Title Page

Abstract | Introduction

Conclusions | References

Tables | Figures

◄ | ►

◄ | ►

Back | Close

Full Screen / Esc

Printer-friendly Version

Interactive Discussion

where $f = e^{-\sigma^2}$ accounts for the partial coherence of the signal. σ is the standard deviation of the phases, defined as $\sigma = \rho x = \rho \frac{2\pi a}{\lambda}$, with a the radius of the particle, and ρ is a roughness parameter, defined as a scaling factor over the size discrepancies: for a given particle of mean size $\bar{x}$, a rough surface entails a possible measurement x of its size through the use of statistical formula of expression

$$x = \bar{x}\,(1 + \rho\delta) \tag{12}$$

where δ is a statistical distribution of standard deviation 1 (Drossart, 1990).

We retain this approach in the present study.

2.2.2 Diffraction by an irregular particle

As for the calculation of the diffracted fields by an irregular particle, we used a Monte-Carlo algorithm. The particulate is considered to be of size x, a variable which is assigned a random value in the distribution described by Eq. (12). The corresponding diffracted field is simply calculated assuming a spherical shape of size x, at an angle θ:

$$S_1^d = S_2^d = x^2 \frac{J_1(x\sin\theta)}{x\sin\theta} \tag{13}$$

The derivation of this result can be found for instance in (van de Hulst, 1957), and represents no more than the well known fact that the Fraunhofer diffraction pattern of a circular aperture (here, the cross section of the particle) is expressed through the use of a Bessel function of first order.

By repeating this calculation a large number of times, one yields a mean diffracted intensity $I^d(\theta)$ which accounts for the various projected sizes of the irregular particle within the light beam. This statistical approach is motivated by the fact that experimental data are averaged over multiple single-particle measurements.

Light scattering at small angles by irregular particles

T. Lurton et al.

Title Page

Abstract | Introduction

Conclusions | References

Tables | Figures

◄◄ | ►►

◄ | ►

Back | Close

Full Screen / Esc

Printer-friendly Version

Interactive Discussion

2.3 Synthesis for irregular particulates

Following Drossart (1990), we operate a weighting process to account for the forward direction coherence: the diffraction approximation is met within a solid angle $\theta = \frac{\sigma \beta_1}{0.1x}$ where $\beta_1 \approx 3.83$ is the first zero of the J_1 Bessel function. Within this angle, only the diffracted parts of our calculation are retained.

Such a theoretical approach must be validated by experimental data. In the following section, we detail an experimental device used for that purpose.

3 Experimental studies

3.1 Description of the experimental device

The device used to gather the experimental data in this study basically consists in a particulate chamber illuminated by a laser beam ($\lambda = 635$ nm) having a power of 25 mW, and an optical canal at the end of which a photodiode gathers the light scattered. This canal is set up at a scattering angle of around 15°, with the angular field of view of the photodiode lying between 13.8 and 16°. The lower angular limit is defined to avoid direct view of the laser beam in the field of view. The upper limit marks the angular domain where the scattered light becomes sensitive to the particulates' nature (Renard et al., 2010). No lenses were used to gather the scattered light; scattered photons travel directly to the photodiode, which presents a diameter larger than the optical canal.

The particulate chamber is such that one single particle passes through the light beam at a time. Basic schematics of the device can be found in Fig. 1. The experimental device can provide counting in 20 classes. The classes are defined by thresholds (in mV) which are chosen during the session of measurements.

The present article focuses mainly on irregular particulates; as a consequence, the uncertainty over measured sizes is naturally high: the "size" of the particulate is all

a matter of definition, be it projected or equivalent diameter. Thus, a degree of uncertainty over the measured particle size is, as a matter of fact and to our knowledge, inherent to each and every OPC. Here, our technique of measurement considers equivalent diameter.

3.2 Samples used for experiments

Our study is based on a set of data gathered over a large variety of particulates: latex beads (in the 0.1–2 µm range), glass beads (in the 5–20 µm range), and sands, salts, carbons, corundum, and volcanic ashes (in the 5–100 µm range). Latex beads are likely to be perfectly spherical, and are supposed to reproduce accurately the Mie solution, whereas the rest of the samples represent a variety of irregular particulates. (Note that we also consider glass beads as semi-irregular, since they can easily be misshapen or broken.)

For the measurement of latex beads, which are provided in liquid medium, we have used the aerosol generator TOPAS ATM 220. Latex beads are diluted in "pure" water. The aerosols travel in a chamber containing highly hydrophilic Silica Gel beads, to remove the droplets and water around the beads. Nevertheless, submicronic solid and liquid residuals remain in the air that is injected in the optical counting system, which could bias the calibration. Also, even if a cleaning procedure of the system is performed after each session of measurements, some latex beads used for previous measurements could remain in the aerosol generator system. We use a differential method for the measurement analysis. First, a reference measurement is carried out using only pure water. Then, this measurement is subtracted from the latex bead measurements. If the contamination is too strong, we can also subtract the measurements obtained previously with beads having smaller diameters. The highest value of the counting (or concentrations) provides the threshold in mV for a given size of beads. Figures 2 and 3 present examples of measurements after applying this procedure.

The calibration for irregular particulates larger than 5 µm is also conducted by a differential method, to remove the contribution of the smaller particulates. For all samples,

Light scattering at small angles by irregular particles

T. Lurton et al.

particulates with different diameters are obtained by using sifters (meshes of 5, 10, 25 and 32 µm in diameter). Concentrations at a given size are retrieved from the measurements by subtracting those at the size below. Figure 4 presents the result for volcanic ashes through a 25 µm sifter. Two maxima of concentration are present. The first one is assumed to correspond to concentrations of particulates having a diameter D smaller than the sifter meshes. The second one is assumed to represent particulates having a diameter smaller to the diagonal $D\sqrt{2}$ of the meshes. Thus, it is possible to retrieve two calibration values of flux vs. size for each sifter by considering the value of the flux at the end of the maxima.

For glass beads, we considered the size distribution provided by the manufacturer instead of the mesh size (the sifters are only used to remove pieces of broken beads and aggregates). For particulates around 100 µm of diameter (silicon carbide), we have considered the size distribution provided by the manufacturers. Thus, the relation between flux and size was derived by considering the position of the maximum concentration distribution.

Results for particulates of different nature (minerals, carbons, salts) are averaged together to study the possible dependence of scattered flux. Figure 5 shows the scattered intensities for several sizes of particulates and for different natures of particulates. As expected, the dispersion is very low, proving the independence of the scattered intensity with regard to the particulates' nature at such low scattering angles.

3.3 Estimation of the experimental roughness parameters

This paragraph aims to establish the link between the theoretical model previously presented and the real set of data gathered through experiments. In order to quantify the roughness parameters of solid particulates, values were calculated from direct analysis of microscope images of the particulates. For each cross-section delineated on a picture, the centre of gravity was determined, and the statistical distribution of the distances between points of the edge and the centre was calculated; an average over the distribution gives a mean radius, and a simple standard deviation calculation yields

Title Page

Abstract | Introduction

Conclusions | References

Tables | Figures

◀ | ▶

◀ | ▶

Back | Close

Full Screen / Esc

Printer-friendly Version

Interactive Discussion

the roughness parameter ρ (see Eq. 12). The operation was reiterated over a large number of particulates for each sample. Table 1 displays the results calculated.

3.4 Numerical simulation results and comparison with measurements

Figure 8 displays the results of a series of simulations performed using the method described in the previous paragraphs. The geometry used was chosen to fit that of the experimental device presented: the light scattered by the particulates ($\lambda = 635$ nm) is received under an angular aperture of 2.2°, at a low centre scattering angle (15°). The simulation results are directly compared to the measured values.

The types of particulates used for the measurements are twofold: on the one hand, latex beads of size less than 2 µm, which are expected to match the Mie theory, and on the other hand irregular particulates of size greater than 2 µm, for which no particular smoothness can be assumed. Largely overlapping sets of data (i.e. both rough and smooth particulates of the same size ranges, in particular over large sizes) are to our knowledge not easily achievable. The ATM aerosols generator cannot work for beads greater than 2 µm. Above that limit, powders can be generated with other kinds of generator and carried to the aerosol counting device through air flow, but they present a risk of possibly being agglomerated and it is difficult to maintain the largest particulates suspended in air without any undesired orientation effects (Daugeron et al., 2006).

For each size of rough particle, given the weak dispersion already demonstrated, a single value was calculated, corresponding to the average scattered intensity of the whole variety of rough particulates studied. Error bars are presented in both dimensions.

For simulation, particulates of refractive index $m = 1.59$ were assumed as a starting point; this value corresponds to the precise index of the regular latex beads used in the lower size range of our measurements. Firstly, the theoretical Mie scattered fluxes were calculated, upon the angular interval [13.8°; 16°] which is that captured by the photo-

diode, with the addition of the identified 18 mV offset upon the scattered intensities, corresponding to the electronic offset of the instrument.

Following this first step, some different roughness parameters were introduced in the model, ranging from 10^{-3} to 0.01, in order to simulate the detection of real, rough particulates. As one can identify in Fig. 8, the larger the roughness parameter, the more severe the discrepancy induced with respect to Mie theory; this affects both the overall scattered intensity – which lowers as the roughness parameter grows – and the trend in the slope of the intensity vs. diameter. Note that the simulated intensities in the roughness model are only displayed for particle sizes greater than twice the wavelength used; as a matter of fact, the roughness of the particulates cannot be seen under that limit. Therefore, the Drossart model, though consistent with the Mie theory under the 2-λ limit, does not make real physical sense for those particle sizes. Note that in Fig. 8 a slight smoothing of the curves was performed, over $\frac{1}{50}$ of the total size range.

As shown in Fig. 8, there is a perfect agreement between model and measurements for the smallest sizes. On the other hand, the scattered flux for irregular solid particulates is lower than the classical Mie solution would predict for regular particles of the same size; the irregular particles measurements are nonetheless reproduced by the roughness model.

Figure 8 also shows that a lower saturation limit is quickly reached when increasing the roughness parameter. Regardless of the refractive index parameter, we can estimate that the saturation regime in our precise geometrical set-up is encountered for $\rho \geq 0.01$. As a matter of fact, this saturation regime corresponds to a preponderant diffraction effect of the particulates; as the refractive index does not play any role in the diffraction process, it is understood that the scattering flux data of all types of particulates shall collapse on the same curve. The above-mentioned saturating roughness parameter value is relatively low; it is very easily met by any kind of irregular particle found in the atmosphere (see Table 1). The fact that the diffraction part is the main contribution to the scattering process for large and rough particles has already

Light scattering at small angles by irregular particles

T. Lurton et al.

Title Page

Abstract | Introduction

Conclusions | References

Tables | Figures

◄ | ►►

◄ | ►

Back | Close

Full Screen / Esc

Printer-friendly Version

Interactive Discussion

been utilised by studies such as (Ulanowski et al., 2012), in which the size of complex-shaped particulates is retrieved through the estimation of diffraction patterns.

Glass beads present an intermediate behaviour, plotted between the standard Mie solution and the roughness model. This is wholly coherent with the expected surface state of glass beads: they are supposed to be fairly smooth, possibly presenting a broken surface, some agglomeration or being misshapen (this can be noticed on Fig. 6). Their roughness parameter should thus be low, though not perfectly null (see Table 1 for a numerical estimation of the roughness parameter of glass beads.) Note for completeness that the refractive index of the glass beads used ($m = 1.56$) is close to the 1.59 assumed for the simulations. As a matter of fact, running the simulation taking into account this slight parameter difference does not yield major changes: Mie oscillations undergo a minor shift, but the intensities for middle-sized particulates remain unchanged.

We have also ascertained, through numerical simulation, that the larger the angular aperture, the less marked the flux discrepancy effect, or put in different terms: the larger the aperture, the higher the roughness parameter needed to lead to saturation. Because we are restraining ourselves to a narrow field of view for experimental studies, these results shall not be presented thoroughly here, but could constitute some interesting matter for further studies.

4 Discussion

A direct interest of this study is that, due to the small scattering angle and angular aperture, the decrease in the intensities for large sizes of particulates naturally entails a broader dynamic range over the measurements: it becomes possible to monitor a wider range of particle sizes whilst relying on a single photodiode and electronics device. The geometry of our measurements has reduced by a factor 10 the intensity of light scattered for the largest particulates (100 µm) with respect to the classical Mie

Light scattering at small angles by irregular particles

T. Lurton et al.

Title Page

Abstract | Introduction

Conclusions | References

Tables | Figures

Back | Close

Full Screen / Esc

Printer-friendly Version

Interactive Discussion

theory. This opens up the possibility to detect larger particulates than using standard aerosol counters, whilst also detecting the smallest aerosols near 0.2 µm.

In our experimental procedure, we were required to choose a compromise between the accuracy of size determination for the smallest particulates and the dynamics of the diameter range. The accuracy is approximately ±0.05 µm for diameters below 1 µm in our laboratory measurement device. Obviously, the accuracy of size determination for the smallest particulates can be improved by increasing the power of the light source. A 100 µm particulate illuminated by light source of 100 mW would provide a scattered flux converted to a voltage of 4 V, which would be close to the saturation limit of a conventional detector and electronics. In this case, the accuracy of the size determination for the submicronic aerosols would be increased by a factor 4.

5 Conclusion

We have investigated the behaviour of light scattering by rough, natural particulates of all sizes (0.1 to 100 µm) at a small scattering angle, and monitored under a narrow field of view. Discrepancies with the classical Mie solution are found, with scattered intensities showing lower values (up to an order of magnitude for the largest particulates) than expected by the classical Mie model. These differences were attributed to the natural roughness of the particulates. A light coherence model was adapted and used to retrieve the intensities measured, through the means of numerical simulation. Good agreement was found between simulations and measured data. As for the roughness parametrisation, it was found that a relatively small roughness parameter caused the scattered intensities to collapse on a lower saturation limit corresponding solely to the diffraction part of the scattered light. This confirms the low dispersion in the scattered intensities observed for different kinds of particulates in the experiments. As this saturation limit is likely to be met even for very slightly rough particulates, the power law observed for large particle sizes can be reasonably used to estimate the sizes for any sort of real particulates.

A direct interest of this study is the conception of versatile scattering measurement devices: given the fact that the measurement dynamics are increased by the angular set-up, one can monitor a broad range of particle sizes (e.g. from 0.1 to 200 µm) whilst relying on a single model of photodiode and electronics. This will in particular be used for the new Light Optical Aerosol Counter (LOAC) which will be soon launched under all types of balloons or used at ground.

The publication of this article
is financed by CNRS-INSU.

References

Brunekreef, B. and Holgate, S. T.: Air pollution and health, Lancet, 360, 1233–1242, 2002. 7566

Cachorro, V. E. and Salcedo, L. L.: New improvements for Mie scattering calculations, J. Elec-tromagnet. Waves, 5, 913–926, 1991. 7569

Daugeron, D., Renard, J.-B., Gaubicher, B., Couté, B., Hadamcik, E., Gensdarmes, F., Basso, G., and Fournier, C.: Scattering properties of sands, 1. Comparison between different techniques of measurements, Appl. Optics, 45, 8331–8337, 2006. 7576

Deshler, T., Hervig, M. E., Hofmann, D. J., Rosen, J. M., and Liley, J. B.: Thirty years of in situ stratospheric aerosol size distribution measurements from Laramie, Wyoming (41° N), using balloon-borne instruments, J. Geophys. Res., 108, 4167, doi:10.1029/2002JD002514, 2003. 7567

Dick, W. D., McMurry, P. H., and Bottiger, J. R.: Size- and composition-dependent response of the DAWN-A multiangle single-particle optical detector, Aerosol Sci. Technol., 20, 345–362, 1994. 7567

5 Donateo, A., Contini, D., and Belosi, F.: Real time measurements of PM2.5 concentrations and vertical turbulent fluxes using an optical detector, Atmos. Environ., 40, 1346–1360, 2006. 7567

Drossart, P.: A statistical model for the scattering by irregular particles, Astron. Journal, 361, L29–L32, 1990. 7570, 7571, 7572, 7573

Eidhammer, T., Montague, D. C., and Deshler, T.: Determination of index of refraction and size
10 of supermicrometer particles from light scattering measurements at two angles, J. Geophys. Res., 113, 206–224, 2008. 7567

European Parliament: Directive 2008/50/EC of the European Parliament and the Council of 21 May 2008 on ambient air quality and cleaner air for Europe, Official Journal, L152, 1–44, 2008. 7567

15 Fischer, S. L. and Koshland, C. P.: Field performance of a nephelometer in rural kitchens: effects of high humidity excursions and correlations to gravimetric analyses, J. Expo. Sci. Env. Epid., 17, 141–150, 2006. 7567

Mackowski, D. W., Altenkirch, R. A., and Menguc, M. P.: Internal absorption cross sections in a stratified sphere, Appl. Optics, 29, 1551–1559, 1990. 7569

20 McMurry, P. H.: A review of atmospheric aerosol measurements, Atmos. Environ., 34, 1959–1999, 2000. 7567

Mie, G.: Beiträge zur Optik trüber Medien, speziell kolloidaler Metallösungen, Ann. Phys., 3, 377–445, 1908. 7567, 7568

Muñoz, O., Volten, H., Hovenier, J. W., Nousiainen, T., Muinonen, K., Guirado, D., Moreno, F.,
25 and Waters, L. B. F. M.: Scattering matrix of large Saharan dust particles: experiments and computations, J. Geophys. Res., 112, 215–232, 2007. 7570

Penttilä, A., Lumme, K., Worms, J. C., Hadamcik, E., Renard, J.-B., and Levasseur-Regourd, A. C.: Theoretical analysis of the particle properties and polarization measurements in the PROGRA2 experiment, J. Quant. Spectros. Ra., 79, 1043–1049, 2003. 7570

30 PROGRA2 website, http://www.icare.univ-lille1.fr/progra2/ (last access: 23 May 2013). 7589, 7590

Renard, J.-B., Brogniez, C., Berthet, G., Bourgeois, Q., Gaubicher, B., Chartier, M., Balois, J.-Y., Verwaerde, C., Auriol, F., Francois, P., Daugeron, D., and Engrand, C.: Vertical distribution

Light scattering at small angles by irregular particles

T. Lurton et al.

Title Page

Abstract	Introduction
Conclusions	References
Tables	Figures

◀ ▶

◀ ▶

Back Close

Full Screen / Esc

Printer-friendly Version

Interactive Discussion

of the different types of aerosols in the stratosphere: detection of solid particles and analysis of their spatial variability, J. Geophys. Res., 113, D21303, doi:10.1029/2008JD010150, 2008. 7567

Renard, J.-B., Thaury, C., Mineau, J.-L., and Gaubicher, B.: Small-angle light scattering by airborne particulates: Environnement S.A. continuous particulate monitor, Meas. Sci. Technol., 21, 085901, doi:10.1088/0957-0233/21/8/085901, 2010. 7566, 7567, 7568, 7573

Rosen, J. M.: The vertical distribution of dust to 30 kilometers, J. Geophys. Res., 69, 4673–4676, 1964. 7567

Ulanowski, Z., Hirst, E., Kaye, P. H., and Greenaway, R.: Retrieving the size of particles with rough and complex surfaces from two-dimensional scattering patterns, J. Quant. Spectrosc. Ra., 113, 2457–2464, 2012. 7578

van de Hulst, H. C.: Light Scattering by Small Particles, John Wiley & Sons, Inc., New York, 1st edn., 1957. 7568, 7569, 7572

Wiscombe, W. J.: Improved Mie scattering algorithms, Appl. Optics, 19, 1505–1509, 1980. 7569

Zemp, E., Elsasser, S., Schindler, C., Kunzli, N., Perruchoud, A. P., Domenighetti, G., Medici, T., Ackermann-Liebrich, U., Leuenberger, P., Monn, C., Bolognini, G., Bongard, J.-P., Brandli, O., Karrer, W., Keller, R., Schoni, M.-H., Tschopp, J.-M., Villiger, N., and Zellweger, J.-P.: Long-term ambient air pollution and respiratory symptoms in adults (SAPALDIA study), Am. J. Resp. Crit. Care, 159, 1257–1266, 1999. 7566

Title Page

Abstract | Introduction

Conclusions | References

Tables | Figures

◀ | ▶

◀ | ▶

Back | Close

Full Screen / Esc

Printer-friendly Version

Interactive Discussion

Table 1. Estimated roughness parameters for some of the samples studied.

Sample	Mean diameter	Estimated ρ
Glass beads	100 µm	6.24×10^{-3}
Sand	85 µm	0.136
Corundum	120 µm	0.151
Volcanic ashes	20 µm	0.173
Salt	310 µm	0.247
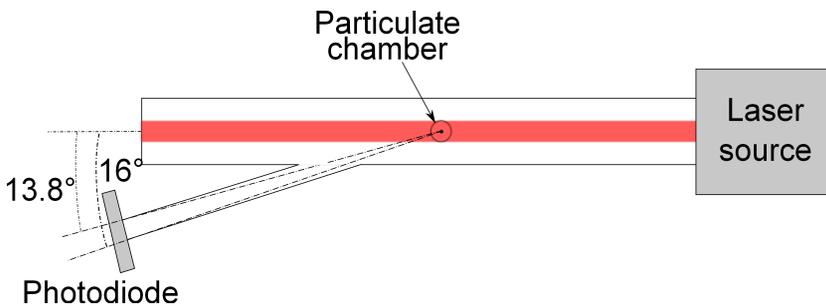
Fig. 1. Basic schematics of the experimental device used.
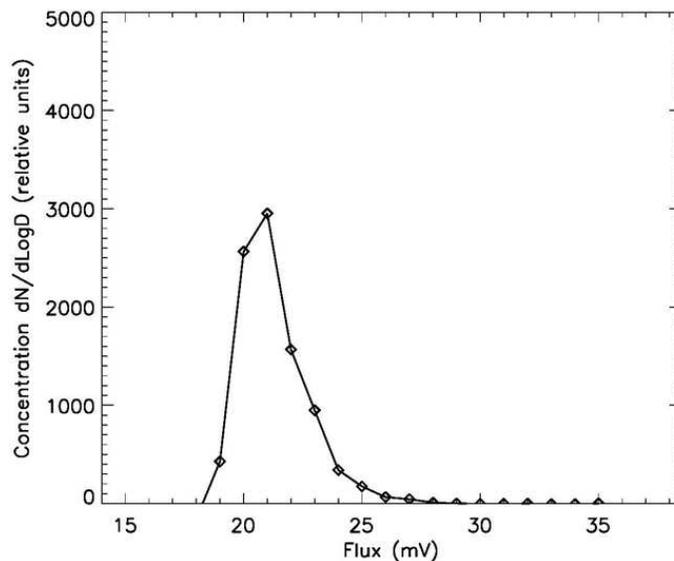
Fig. 2. Measurements for latex beads of 400 nm.
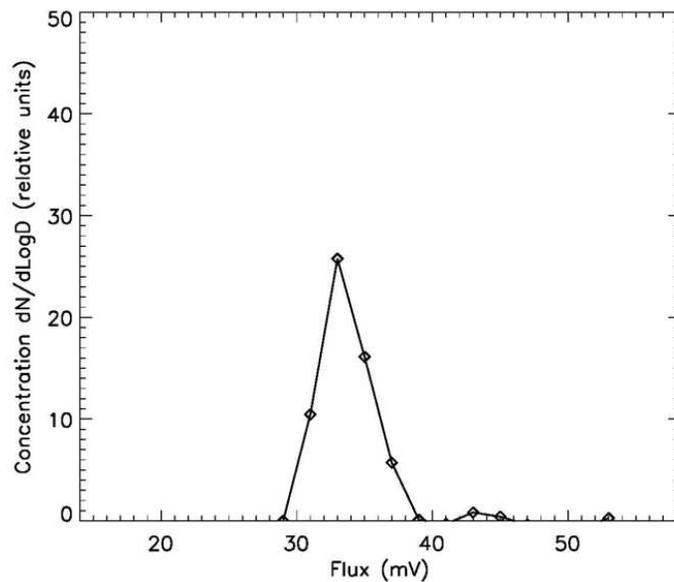
Fig. 3. Measurements for latex beads of 900 nm.
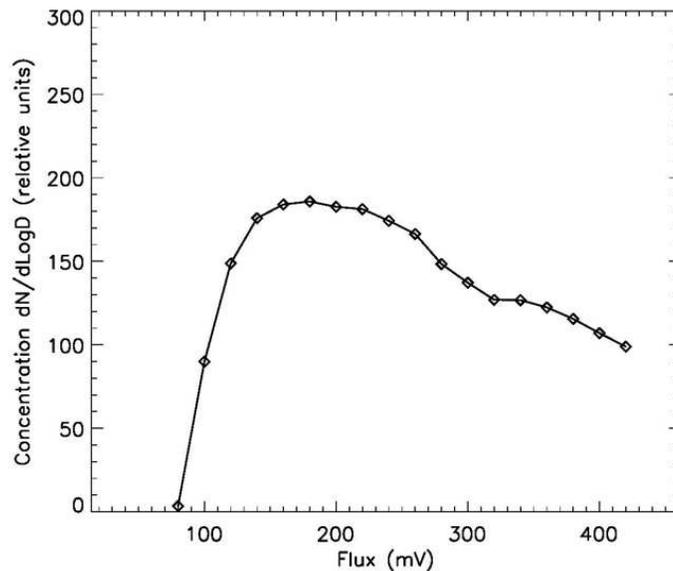
Fig. 4. Measurements for volcanic ashes through a sifter of 25 μm (after subtracting the measurement through a 10 μm sifter).
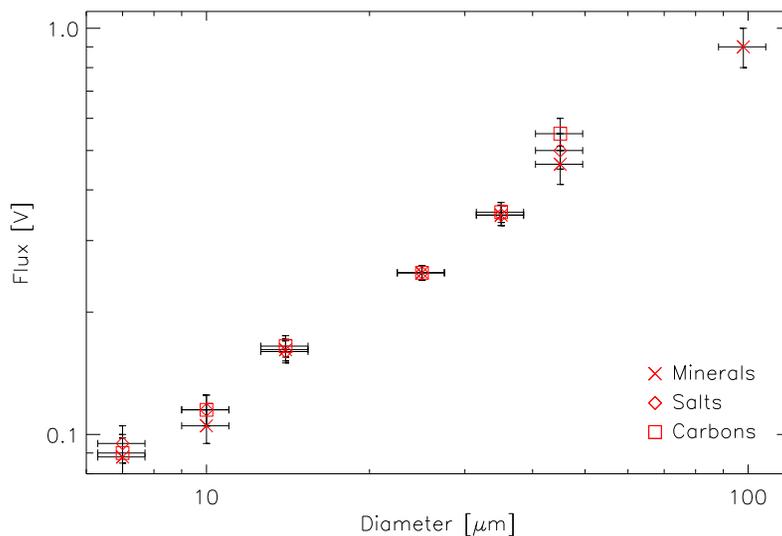
Fig. 5. Scattered intensities for different types of particulates.
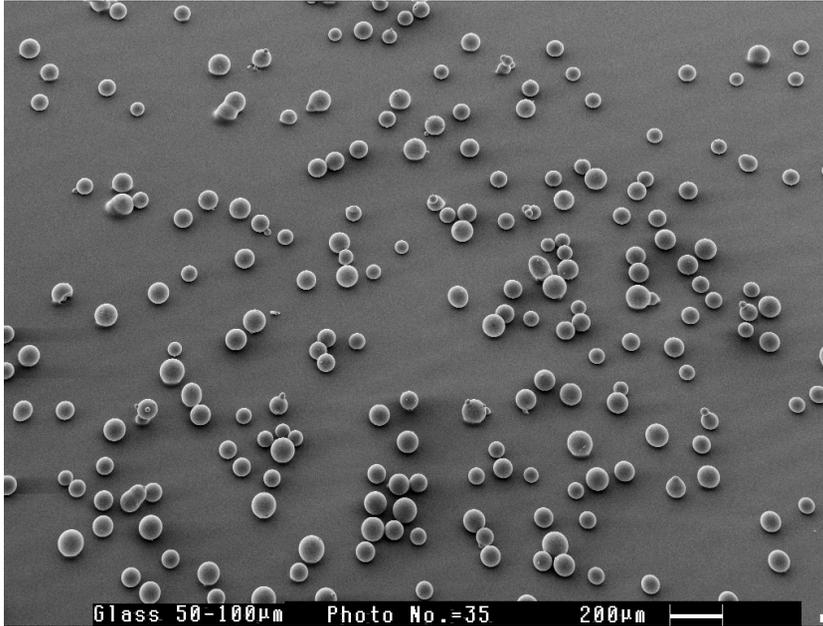
Fig. 6. Picture of glass beads used for the experiments (source: PROGRA2 database (pro, 2013)).
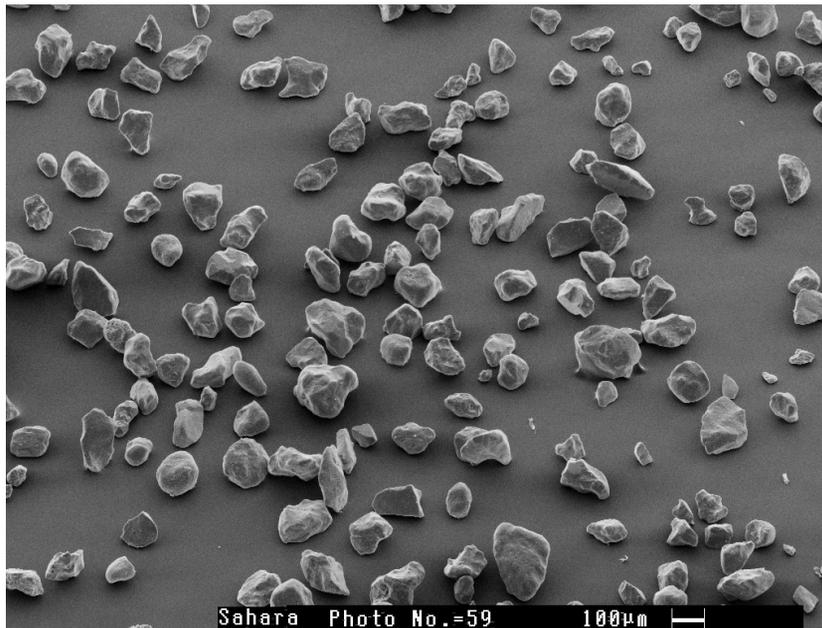
Fig. 7. Picture of sand grains used for the experiments (source: PROGRA2 database (pro, 2013)).
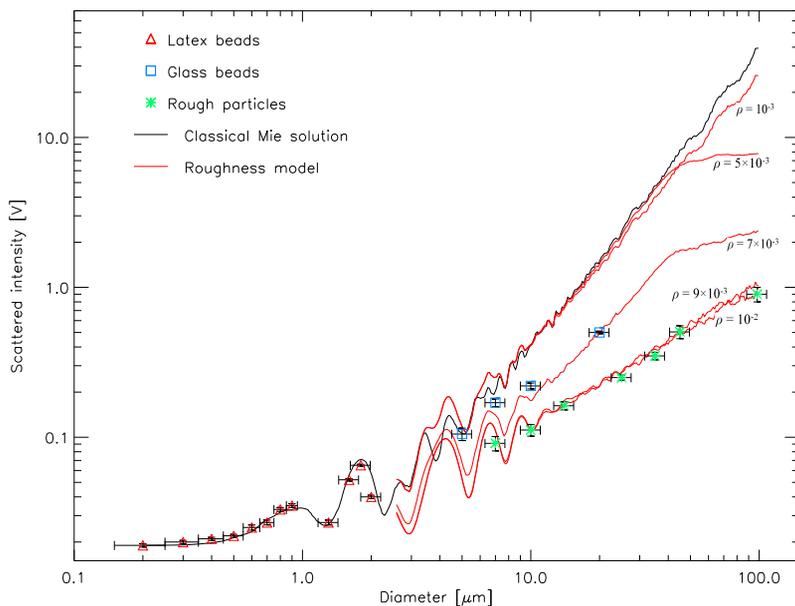
Fig. 8. Comparison of measurements for different kinds of particulates with both the classical Mie solution (plain black line) and the roughness scattering model, for different roughness parameters (plain red lines). Note that the two curves for $\rho = 9 \times 10^{-3}$ and $\rho = 10^{-2}$ are almost identical, due to the saturation phenomenon explained in the text.